

A new real-time debris flow and snow avalanche detection system based on optical fiber sensing

*Original*

A new real-time debris flow and snow avalanche detection system based on optical fiber sensing / Barla, Marco; Aiassa, Santina; Antolini, Francesco; Insana, Alessandra; Gaudino, Roberto; Rizzelli Martella, Giuseppe; Pellegrini, Saverio. - In: LANDSLIDES. - ISSN 1612-5118. - 22:5(2025), pp. 1367-1382. [10.1007/s10346-024-02399-2]

*Availability:*

This version is available at: 11583/2995912 since: 2025-07-17T06:25:54Z

*Publisher:*

Springer

*Published*

DOI:10.1007/s10346-024-02399-2

*Terms of use:*

This article is made available under terms and conditions as specified in the corresponding bibliographic description in the repository

*Publisher copyright*

Springer postprint/Author's Accepted Manuscript

This version of the article has been accepted for publication, after peer review (when applicable) and is subject to Springer Nature's AM terms of use, but is not the Version of Record and does not reflect post-acceptance improvements, or any corrections. The Version of Record is available online at: <http://dx.doi.org/10.1007/s10346-024-02399-2>

(Article begins on next page)

# A new real-time debris flow and snow avalanche detection system based on optical fiber sensing

Marco Barla<sup>a</sup>, Santina Aiassa<sup>b</sup>, Francesco Antolini<sup>\*b</sup>, Alessandra Insana<sup>a</sup>, Roberto Gaudino<sup>c</sup>, Giuseppe Rizzelli Martella<sup>c</sup>,  
Saverio Pellegrini<sup>c</sup>

<sup>a</sup> Department of Structural, Building and Geotechnical Engineering (DISEG) - Politecnico di Torino, Corso Duca degli Abruzzi 24, 10129, Torino (Italy).

<sup>b</sup> Geosolving srl, Corso Orbassano 336, 10137 Torino (Italy).

<sup>c</sup> Department of Electronics and Telecommunications (DET) – Politecnico di Torino, Corso Duca degli Abruzzi 24, 10129, Torino (Italy).

\* Corresponding author: [francesco.antolini@geo-solving.com](mailto:francesco.antolini@geo-solving.com), Tel: +39 328 5421340

## Abstract

This paper presents a novel real-time detection and early warning system for debris flow and snow avalanches based on distributed optical fiber sensing called Optialp. The functioning principle of the system is based on detecting the vibrations and the impacts generated by the propagation of these phenomena in a spatially continuous way through the real-time analysis of the polarization variations along the optical fibers. A prototype of the system was extensively tested through an experimental laboratory setup reproducing a slope to scale. A series of tests were carried out emulating mass movements. Data recorded from all the tests were used to develop a new algorithm based on a threshold value and a moving average filter capable of distinguishing the signals related to the emulated mass movements from all the further noisy signals. The algorithm was integrated into a prototype of a fiber optic interrogator which performs the real-time analysis of the data acquired and can generate a warning signal whenever mass movements are detected. The results obtained at the laboratory scale have revealed that the technique could precisely, simply, and rather economically identify the polarimetric perturbations induced on the optical fibers by external forces. The laboratory results are promising and suggest that the optical fibers embedded into the ground along one or more sections of the channels where the debris flows or snow avalanches propagate can be used as a novel distributed detection and early warning system, improving the current technologies typically based on discrete monitoring points and sensors.

**Keywords:** Early Warning, Debris Flow, Snow Avalanche, Detection, Distributed Optical Fibers.

## 1 Introduction

In the last years, the frequency and the spatial distribution of rain and snow precipitation have drastically changed in many areas of the world accompanied by a simultaneous increase in the frequency of intense phenomena (IPCC 2023; EEA 2017; Stocker et al. 2013, Insana et al. 2021). Debris flows and avalanches are natural phenomena occurring as a consequence of intense or prolonged rainfalls and snowfalls propagating along river catchments and slopes in mountainous regions. Despite the intrinsic differences among the materials involved as well as the different mechanical and rheological features, the commonalities of both these two mass-moving phenomena are:

- the capability to move very quickly i.e. 10 m/s and more (Arattano and Marchi 2005; Bertolo and Wieczorek 2005; Gauer 2014; Havens et al. 2014; Prochaska et al. 2008; Rammer et al. 2007);
- the capability to travel for long distances i.e. up to some km (Butler and Malanson 1992; Hungr et al. 2014; Iverson 1997; Jakob 2005; McClung and Schaerer 2006; Schweizer et al. 2021) from the point where they originate which generally corresponds to the upper portion of a catchment basin or a slope;
- the capability to entrain further materials (soils, rocks, trees) through erosion of the channels and the slopes during the movement;
- their intermittent (or sporadic) occurrence as a consequence of intense rainfalls and snowfalls i.e. prolonged inactivity followed by a sudden recovery;
- a generally high destructive power.

Although the frequency of occurrence of debris flows and avalanches show differentiated trends in different basins that are not easily generalized to a larger scale (Beniston et al. 2011; Bigano and Pauli 2007; Marchi et al. 2002; Pelfini and Santilli 2008; Sass and Oberlechner 2012; Stoffel and Huggel 2012), this frequency in the anthropized basins like the Alpine ones is sufficient to create conditions of high risk for people settlements, road, railways as well as other linear infrastructures exposed to risk. To mitigate this risk, non-structural measures, i.e., monitoring and Early Warning Systems (EWSs) are assuming greater importance thanks to the growing reliability of sensors and transmission systems and their relatively low cost. The aim of the non-structural measures for the mitigation of debris flows and avalanches here considered is primarily to generate timely alarms to be sent and dispatched to all the stakeholders and to the elements exposed to risk through the real-time and continuous observation of physical quantities which characterize the observed phenomenon. A crucial aspect of an EWS is therefore the selection of the most useful quantities to be observed and measured. In this framework, different monitoring systems and techniques for debris flows and avalanches have been proposed (Aaron et al. 2023; Antolini et al. 2019; Arattano and Marchi 2005; Belli et al. 2022; Hurlimann et al. 2019; Itakura et al. 2005; Leonardi et al. 2021; Nagl et al. 2022). Such techniques comprise ultrasonic, radar, and laser sensors for measuring the height of the flow along the channel and the velocity field, seismic and sonic sensors to identify and measure the dynamic effects related to the occurrence and propagation of the mass movements, load cells, force plates, entrainment sensors, sensors for measuring the interstitial pressure of the soil, sensors for identifying the passage of the snow/debris flow or directly installed in the channels where these phenomena usually propagate (trigger lines, wire sensors, pressure sensors, pendulums, clinometers) as well as weather stations to measure the precipitation, video cameras that have more general use, and strain transducers on mitigation structures. In the last years, some remote sensing techniques like the Doppler radar (Gauer et al.

67 2007; Rammer et al. 2007) and the infrasonic sensors (Thuring et al. 2015; Ulivieri et al. 2011) have also been developed  
68 to detect the surface velocities or the air pressure fluctuations related to the occurrence of snow avalanches. The extreme  
69 variability of the types of sensors adopted can be noted as well as the fact that no fiber optic system is generally reported  
70 in the literature for the monitoring of such phenomena nor for EWS applications.

71 The applications of optical fibers for geohazard and geoenvironmental monitoring applications date back about 25 years  
72 with the attempts at the spatially continuous measurement of some physical parameters such as temperature, deformations,  
73 and water content inside earth embankments (Aufleger et al. 1997; Johansson et al. 2000; Beck et al. 2010), followed by  
74 applications for monitoring in-depth deformations (Michlmayr et al. 2017; Schenato 2017). Meanwhile, different optical fiber  
75 technologies have been developed for geohazard and structural monitoring such as the Optical Time Domain Reflectometry  
76 (OTDR), the Optical Frequency Domain Reflectometry (OFDR) both based on Rayleigh, Raman or Brillouin backscattering  
77 and the Fiber Bragg Grating (FBG). A more detailed description of the working principles of these techniques is outside the  
78 scope of this paper and can be found in Bao and Wang (2021), Bolognini et al. (2009), Hong et al. (2016), Motil et al. (2016).  
79 These technologies can be further subdivided into three classes: point, quasi-distributed, and fully-distributed fiber optic  
80 sensing (DFOS). The main characteristics, advantages and disadvantages are (Wang et al. 2023):

- 81 - point sensing is characterized by a discrete number of sensors that measure changes in parameters in a small  
82 area near a predetermined point along the optical fiber line. A typical example is the FBG sensor. They can offer  
83 excellent performance in measuring specific locations;
- 84 - quasi-distributed sensing contains multiple sensing units to form a sensor array and enables multi-point sensing.  
85 The system combines the characteristics of single-point sensors and fully distributed sensors;
- 86 - DFOS utilize the fiber to measure physical parameters along its entire length, treating the sensed parameters as  
87 functions of the length of the fiber position. This allows DFOS to continuously monitor the external physical  
88 parameters distributed along the fiber path, while also obtaining the state of the spatial distribution of the measured  
89 physical parameters and their variation over time.

90 For the real-time detection of avalanches and debris flows DFOS are of particular interest. DFOS are capable of spatially  
91 continuous monitoring of the physical parameters of the environment where they are placed, since the “sensor” is made up  
92 of the same fibers or set of fibers concatenated together. The mechanism underlying the measurement, which can exploit  
93 different processes (Rayleigh, Raman, Brillouin scattering or FBG), is based on a sensor that continuously generates optical  
94 pulses that are sent inside the fiber. The variations of the backscattered signal over time measured by the sensor correspond  
95 to variations of the properties of the fiber associated to the change of one or more parameters of the environment where  
96 the optical fiber is installed. Applications aiming at the high accuracy measurement of stresses, strains, displacements,  
97 temperatures, pore water pressures, etc. have been reported in the scientific literature (Inaudi 2014; Lloret et al. 2003;  
98 Michlmayr et al. 2017; Olivero et al. 2018; Schenato 2017; Zhu et al. 2017).

99 The feasibility of the DFOS for the detection of seismic signals related to ice cap microseismicity and more specifically to  
100 snow avalanche occurrence has been demonstrated only in the last few years (Edme et al. 2023; Fichtner et al. 2022;  
101 Hudson et al. 2021). In particular, in the application described by Edme et al. (2023) a Distributed Acoustic Sensing (DAS)  
102 with existing fiber-optic telecommunication cables was used to detect the snow avalanche occurrences in the Swiss Alps.

103 The preliminary results obtained demonstrated that the proposed system was able to identify their occurrence even though  
104 most of them did not reach the fiber optic cable.

105 On the contrary, very few full-scale applications are known to date concerning the detection of debris flow. For example,  
106 Michlmayr et al. (2017) recently confirmed the feasibility of such an approach in the laboratory by carrying out tests in an  
107 inclined chute with a distributed acoustic sensing technology based on optical fiber coils. However, the aim of the study was  
108 the triggering of shallow landslides caused by the occurrence of intense rainfall and not the detection of snow avalanches  
109 and debris flows along a channel. A DFOS-based monitoring system has been developed to measure the impact forces of  
110 debris flows directly by Qin et al (2020) and Tan et al. (2020). Whereas, there are no known applications in the literature  
111 that envisage the use of DFOS as well as their possible interface with radio nodes for early warning purposes.

112 Based on the state of the art, the novelty of the current study lies in the investigation of the use of fiber optics for early  
113 warning purposes against the occurrence of debris flows and snow avalanches. The motivation stems from the need to  
114 tackle the increasing frequency of such events due to climate change and to mitigate the risk for people, structures and  
115 infrastructures (Insana et al. 2021). In the following sections, we will present the characteristics of a new system based on  
116 the use of fiber optics to detect the propagation of mass movements by measuring in real-time the polarization variations  
117 along the whole optical fibers' length together with the result of an extensive laboratory activity aimed at evaluating the  
118 feasibility of such system. A preliminary assessment of the technical and economic feasibility of the system for real scale  
119 applications is also given.

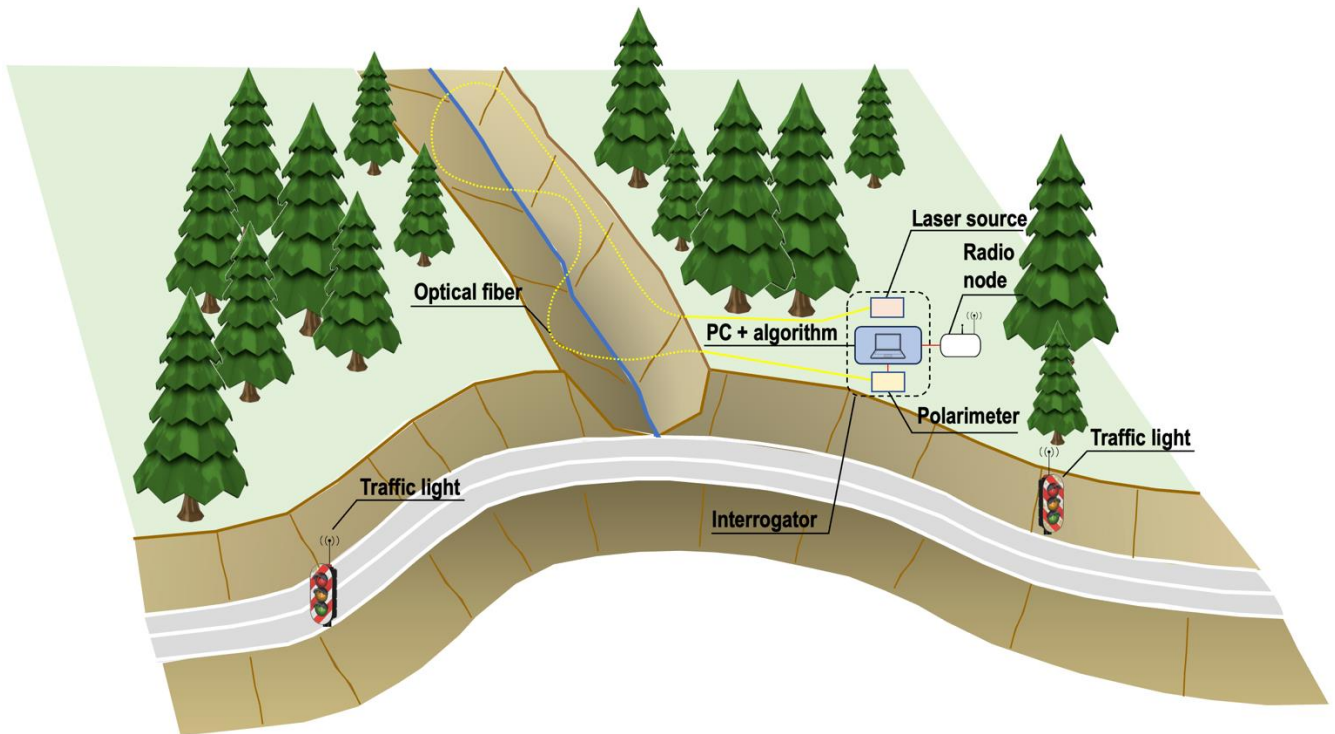
## 120 **2 Characteristics of the system and principle of operation**

121 The system here described has been submitted to patenting on 07/12/2022 under the number 102022000025158 and will  
122 be referred to as Optialp in the following.

123 The proposed system to detect mass movements is composed of one or more optical fibers to be installed at the monitored  
124 site, connected, at one end, to a laser source and, at the other end, to a polarimeter. The polarimeter will measure data  
125 from the optical signal emitted by the laser travelling through the fiber and transfer it to a control unit (a laptop or embedded  
126 microprocessor system running a specifically developed algorithm) that can activate, through a radio node, alarm systems  
127 such as traffic lights or alternative informative devices to convey specific messages to the elements at risk. Figure 1 shows  
128 a schematic layout of the Optialp system in the case of the detection of debris flows and snow avalanches along a channel  
129 or to detect the impacts of rock blocks against a rockfall barrier. The optical fiber is buried into the ground along the channel  
130 by excavating small trenches to be filled after the deployment of the fibers. Alternatively, they can be directly fixed (by  
131 dowels or clamps) to the rock, when present. The first installation mode is more robust, while the second is more prone to  
132 damages in case of events. To monitor rock fall impacts, the fibers are hanged to the steel net of the rockfall barrier. Fibers  
133 are then physically connected to the so-called interrogator which comprises the laser source, the polarimeter and the control  
134 unit.

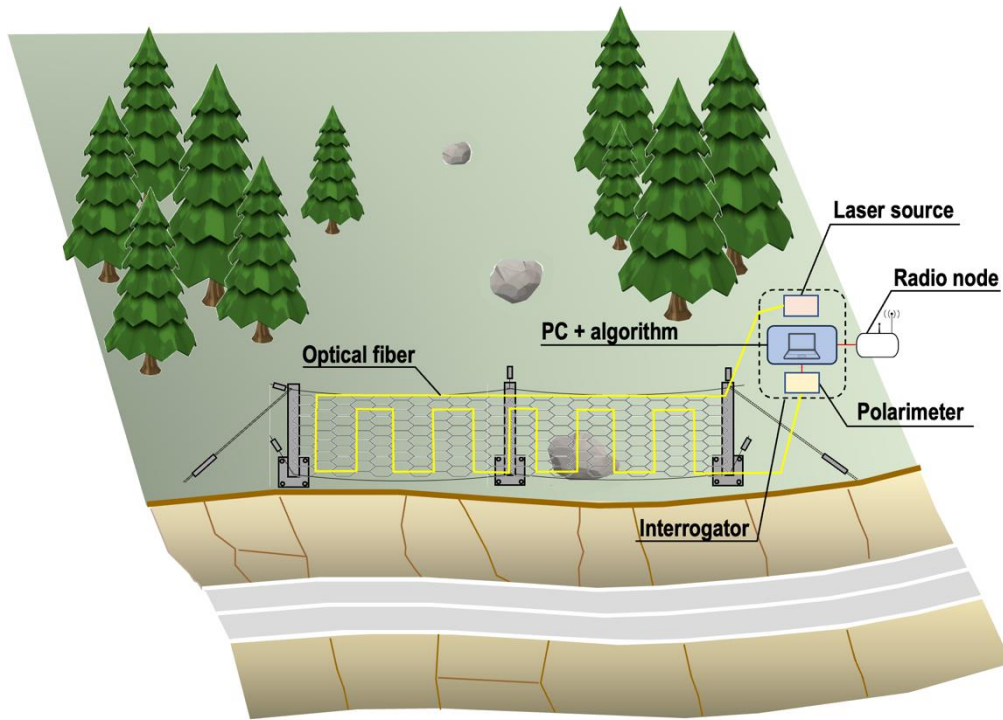
135 The detection principle adopted by the system is given by the state of polarization (SOP) of light propagating inside the  
136 optical fiber. This can be uniquely described in a three-dimensional space by the Stokes vector ( $\vec{S}$ ), identified by the three  
137 Stokes parameters, namely  $S_1$ ,  $S_2$ , and  $S_3$ . The three-dimensional space over which  $\vec{S}$  is identified is the Poincaré sphere

138 and each point on its surface represents a different SOP. The state of polarization at a fiber output is affected by  
139 birefringence (Forman and Jahoda 1988; Kogelnik and Winzer 2012). External stresses acting on the fibers, such as those  
140 generated by mass movements, determine a sudden birefringence variation of the optical material and, consequently, a  
141 variation of the SOP of the light propagating inside the fiber. This change can be detected by monitoring the angular variation  
142 over time of the Stokes vector called the State Of Polarization Angular Speed (SOPAS). To analyse this, allowing the  
143 detection of the physical phenomena occurring, a specific algorithm to be implemented in the interrogator has been  
144 developed by the Authors.



145  
146

(a)



(b)

Figure 1 - Layout of the Optialp system along a gully subjected to debris flows/snow avalanches for road protection (a) and on a rockfall barrier to detect rock blocks impacts (b).

## 2.1 New algorithm for signals processing

The block diagram of the algorithm developed to process the data acquired from the optical fibers through the polarimeter is shown in Figure 2. The different blocks in the diagram, describe the flow of the interpretation process. Particularly:

- the polarimeter collects the time series of the 3 Stokes parameters;
- using the 3 Stokes parameters collected, the SOPAS is calculated at the instant  $k$ ;
- a Finite Impulse Response (FIR) filter is applied that carries out a moving average on the input SOPAS values. The output  $\omega_s(k)$  is therefore the time-averaged series of the input data. To perform this operation, it is necessary to define the size of the buffer that will contain the samples to be averaged. This value is linked to the  $T_{mov}$  parameter, which defines the time duration of the buffer. The greater the moving average window, the greater the buffer to be filled, and therefore the delay introduced in the alarm;
- the output  $\omega_s(k)$  values are compared to the SOPAS threshold  $\omega_{th}$  defined by the user. If the  $\omega_s(k)$  value is higher than the threshold, then the alarm is activated.

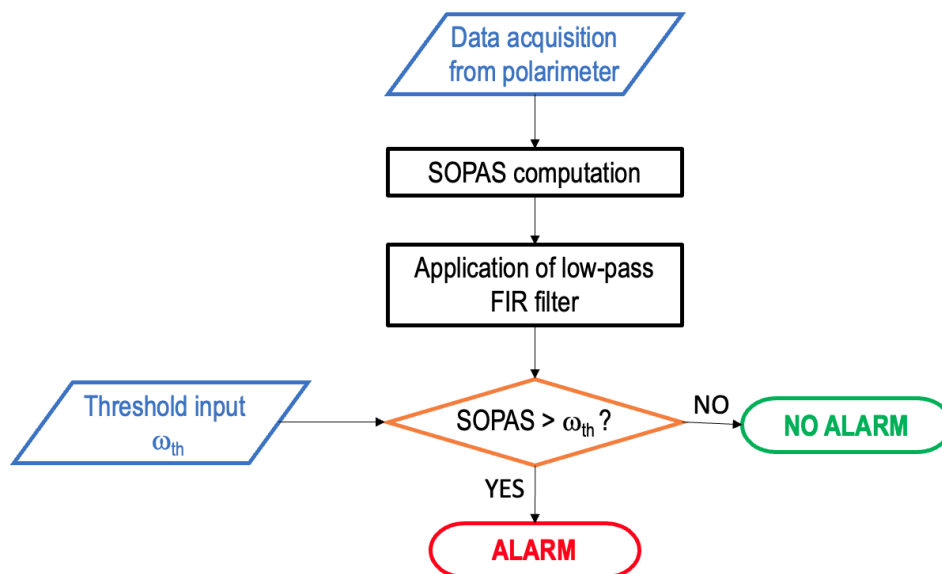


Figure 2 - Blocks diagram of the new algorithm developed to process the signals acquired by the optical fiber and to identify the occurrence of the simulated mass movements.

163

164

165

166 The low-pass Finite Impulse Response (FIR) filter is applied to eliminate the random peaks i.e., the noise of the  
 167 measurements, and to smooth the time series. The duration of the time window ( $T_{mov}$ ) is thus the first free parameter of the  
 168 algorithm. The other free parameter to be considered in the algorithm is a specific SOPAS threshold value ( $\omega_{th}$ ) expressed  
 169 in rad/s. Using different combinations of these two parameters, the output of the algorithm could result in a correct detection  
 170 (CD) of the simulated mass movement, a missed detection (MD) i.e., the simulated event is not detected, or a false alarm  
 171 (FA) i.e., an alarm is triggered but no event has occurred or another event not related to a mass movement has occurred.  
 172 In the latter case, further identification and classification of the signals are needed. The FIR filter and the threshold  
 173 comparison perform a sample-by-sample check of the smoothed SOPAS against the threshold. By increasing the value of  
 174  $T_{mov}$ , the oscillations in the SOPAS time series reduce, but at the same time, this requires a lower threshold value  $\omega_{th}$  to be  
 175 selected to avoid the occurrence of MDs or FAs. The application of higher values of  $T_{mov}$  could also introduce an excessive  
 176 delay in the processing due to the large number of samples contained in the time-moving window. On the contrary, if the  
 177 threshold value is set too high without accounting for this effect, MD cases are likely to happen; a very low value of  $T_{mov}$   
 178 does not remove the noise component from the signals and, if the threshold is set too low, FAs might occur. The optimal  
 179 definition of the two free parameters  $T_{mov}$  and the threshold value (expressed in terms of SOPAS) was then evaluated and  
 180 selected on the basis of the laboratory experimental activity as described in the next chapter.

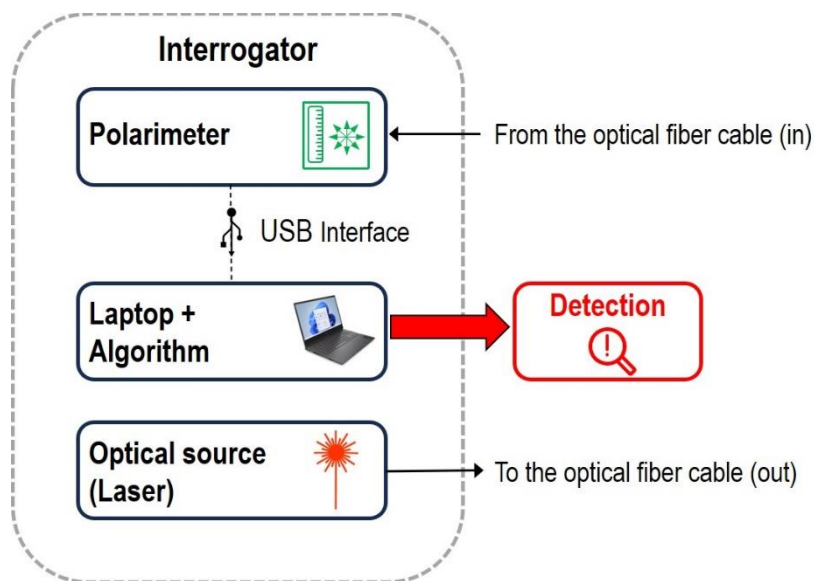
181 An in situ implementation of the optical fiber polarization-based monitoring system would be affected by the external  
 182 environment, e.g. wildlife movements, changing weather conditions, and temperature. Depending on what is considered an  
 183 hazard and on the noise conditions, the threshold and smoothing filter length value need to be set appropriately through a  
 184 calibration period on the noise level associated with non-harmful events. Additionally, these events would not generate  
 185 SOPAS variations overcoming the threshold for an extended period, as debris flow or snow avalanches would. Therefore,  
 186 a simple upgrade of the algorithm, including a check on the time duration should be enough to distinguish between  
 187 hazardous and harmless scenarios, reducing false alarm occurrences (Pellegrini et al., 2024).

188 To further improve the performance of the algorithm, the sampling frequency of the polarimeter was optimized. After a  
189 careful analysis of the acquired data in the frequency domain, it was found that the SOPAS variations had frequency  
190 components up to a few tens of Hz. Because of this, it was possible to downsample the frequency to 95.4 Hz, the lowest  
191 enabled by the polarimeter, therefore reducing the computational effort since this sampling frequency is sufficient to describe  
192 and identify the frequency components of the simulated events.

193 More specific details on the development of the algorithm can be found in Pellegrini et al. (2023, 2024).

## 194 2.2 The interrogator prototype

195 The prototype of the interrogator was obtained by connecting to the optical fiber cable the laser source to one end (out) and  
196 the polarimeter to the other end (in). The polarimeter which measures the SOPAS variation along the fiber circuit is  
197 interfaced to a PC, where a specific MATLAB script is running in real-time, through a USB connection (Figure 3). The  
198 MATLAB script reads with a specific frequency sampling rate equal to 95.4 Hz the Stokes parameters, applies the algorithm  
199 described in section 2.1, displays the SOPAS in real-time and generates a specific signal when the SOPAS threshold value  
200 is exceeded.



201  
202  
203

Figure 3 - Scheme of the fiber optic interrogator prototype adopted in the experimental tests.

204 By coupling the interrogator with a radio node, the output signal generated when the SOPAS threshold is exceeded might  
205 be used in an operational environment to control warning tools such as traffic lights which can be placed along mountain  
206 roads as shown in Figure 1a.

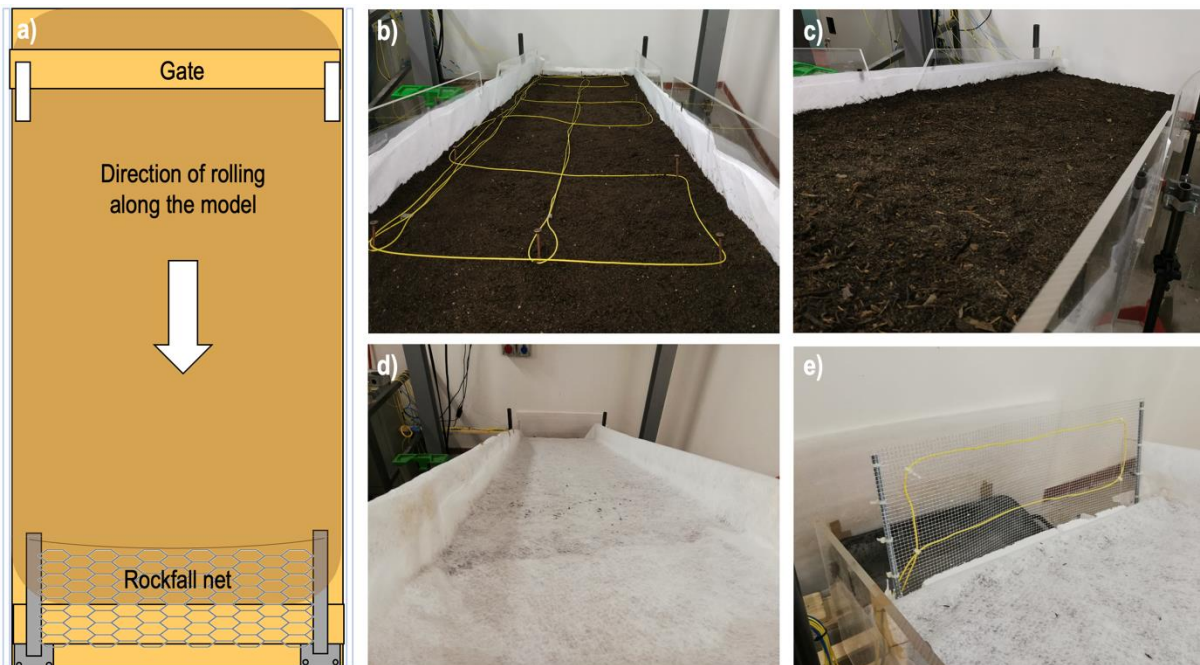
## 207 3 Experimental testing and validation in the laboratory

### 208 3.1 Experimental Setup

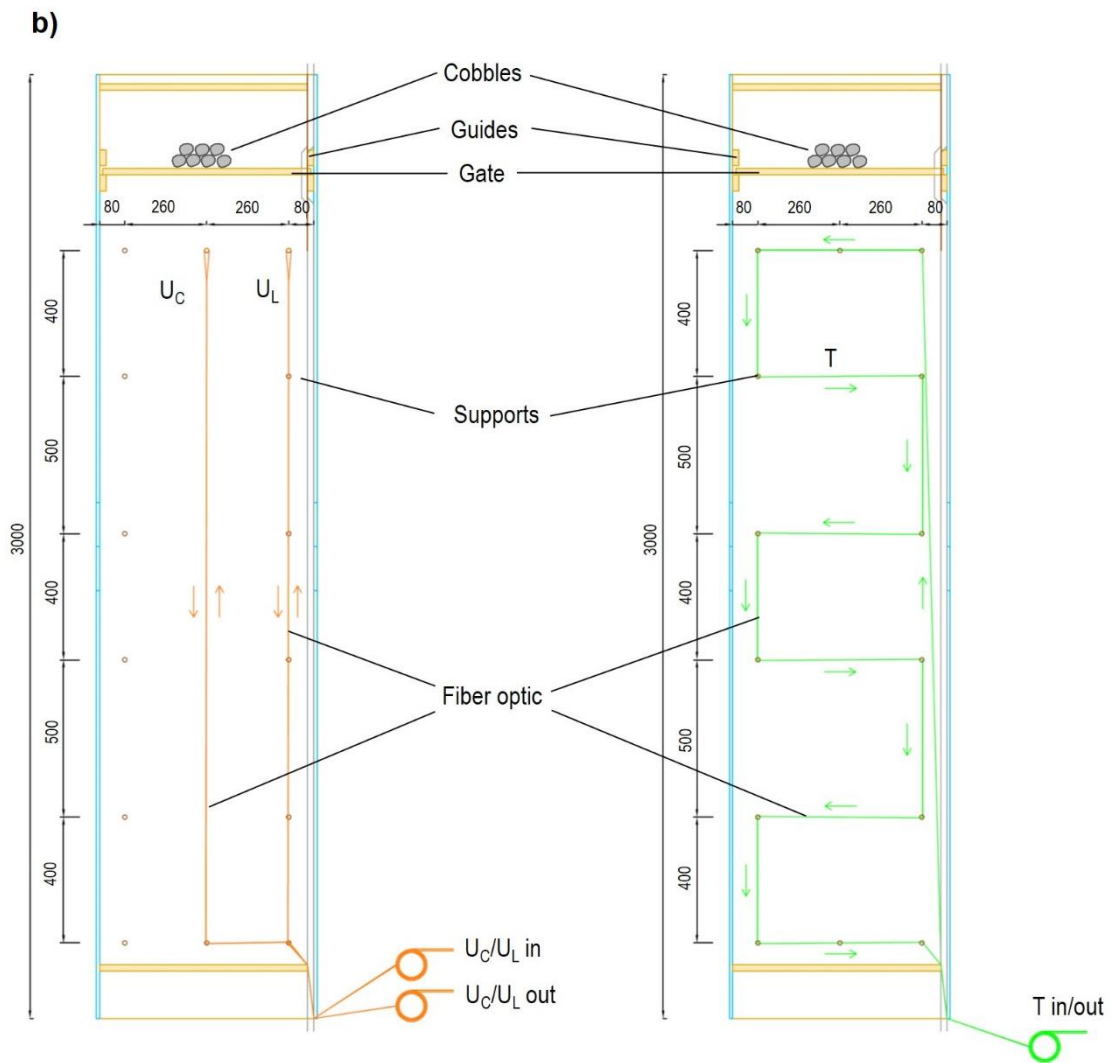
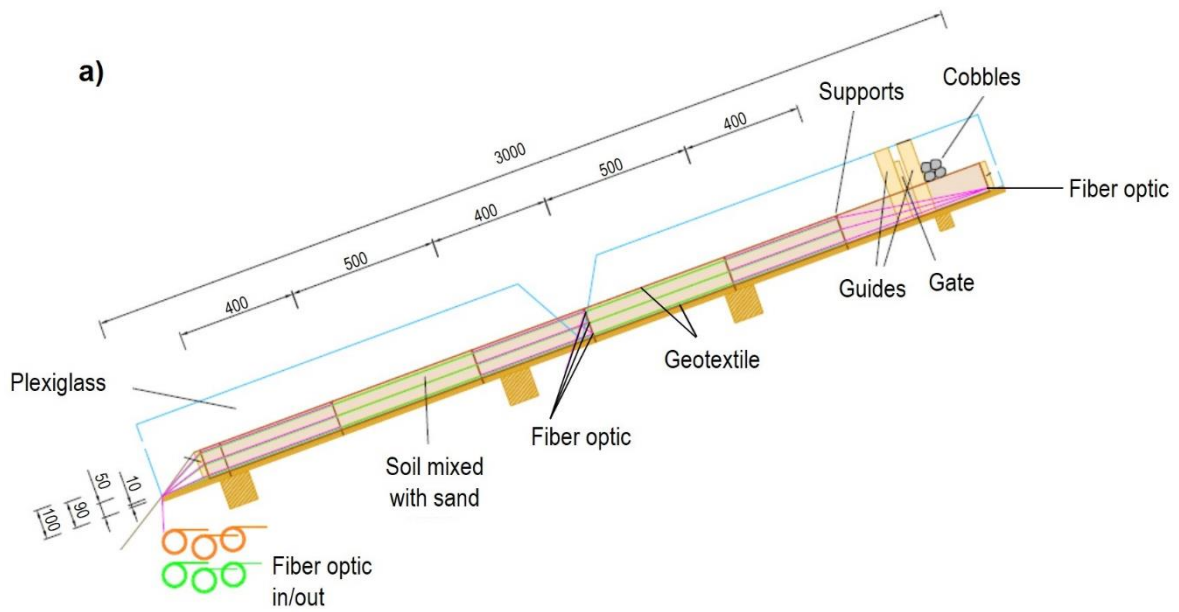
209 To test and validate the potential use of the DFOS for debris flows and snow avalanches detection, a scale model of a  
210 natural slope was reproduced in the laboratory (Errore. L'origine riferimento non è stata trovata.). The model consists

211 of a phenolic plywood base and plexiglass sides with a size of approximately 3 meters in length and 0.7 meters in width.  
212 The plane is made up of two independent parts connected through a series of joint hinges which allow for the independent  
213 inclination of the two portions of the plane designed to simulate more articulated geometric configurations of the slope. For  
214 the experiments carried out, a uniform inclination equal to about  $30^\circ$  was used. A layer of organic soil mixed with sand, with  
215 a total thickness of about 10-12 cm, was placed over the plywood base and inside a geotextile. The latter has the function  
216 of protecting the underlying wooden surface, as well as facilitating the compaction of the soil and sand mixture. Buried in  
217 the soil, single optical fibers were embedded at three different depths (10, 50, and 90 mm) using three different geometric  
218 layouts (Figure 5):

- 219 • Parallel to the maximum slope inclination placed in the middle of the model ( $U_C$ );
- 220 • Parallel to the maximum slope inclination alongside one edge of the model ( $U_L$ );
- 221 • Transversal to the maximum slope inclination with six transversal crossings (T) placed at a distance comprised  
222 between 400 and 500 mm from each other.



223  
224 Figure 4 – Sketch of the experimental setup (a) and pictures of the construction phases: installation of the optical fibers  
225 (b), covering with soil (c), installation of the protective geotextile (d) and installation of the rockfall net equipped with  
226 optical fibers (e).



227

228

229

Figure 5 – Schematic cross section (a) and plan views (b) of the experimental setup highlighting the arrangement of the different optical fibers layouts.

230 Table 1 summarizes the main geometric characteristics of the different fiber optic layouts installed in the model.  
 231  
 232 A series of rigid supports were used to tie the fibers outside the model thus minimizing possible oscillations that could alter  
 233 the measurements. The experimental setup model is completed by a wooden liftable gate installed in the top portion of the  
 234 slope, allowing for the release of different granular materials for simulating mass movements occurring along the slope.  
 235 Each termination of the optical fibers is connected respectively to a laser and a polarimeter placed at a short distance from  
 236 the model. A Fabry-Perot laser emitting light at 1550 nm was used as the optical source for the signal propagating inside  
 237 the single-mode fibers. The optical fibers are then coupled into a laboratory polarimeter (Novoptel PM1000), an instrument  
 238 that allows measuring with a specific sampling frequency  $f_s$  the SOPAS of the light, included in the interrogator prototype  
 239 described in section 2.2. When the SOPAS threshold is exceeded, an acoustic signal is activated and a red light is turned  
 240 on to the PC screen (Figure 6).

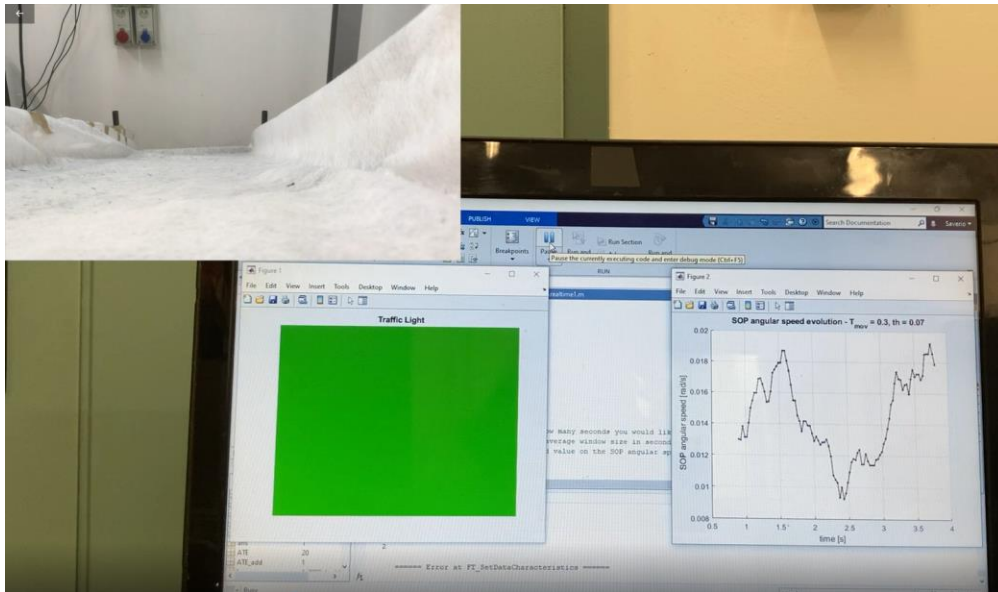
241

242 Table 1 - Summary of the main geometric characteristics and corresponding code of the different fiber optic layouts  
 243 installed in the laboratory scale slope model.

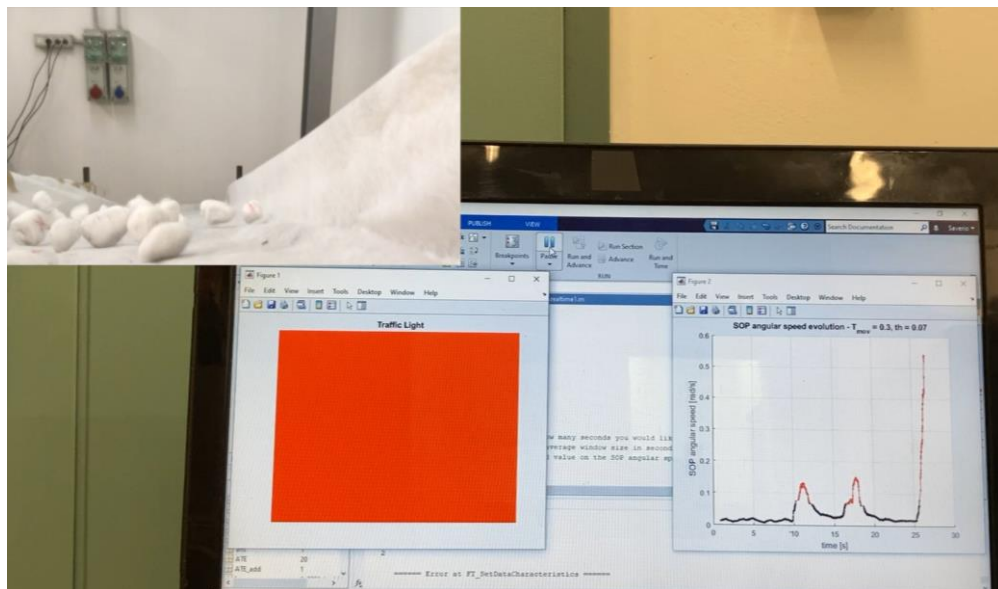
Geometric layout	Depth (mm)	Code
	10	U3 <sub>C</sub>
Parallel to the maximum slope inclination in the middle of the model	50	U2 <sub>C</sub>
	90	U1 <sub>C</sub>
	10	U3 <sub>L</sub>
Parallel to the maximum slope inclination alongside one edge of the model	50	U2 <sub>L</sub>
	90	U1 <sub>L</sub>
	10	T3
Transversal to the maximum slope inclination with six transversal crossings	50	T2
	90	T1
	-	RN1
Rockfall net – simple loop	-	RN1
Rockfall net – meandering loop	-	RN2

244

245



(a)



(b)

Figure 6 – Operation of the optical fibers interrogator and emulation of a traffic light on a PC screen: when operating below the SOPAS threshold value and no events are identified (a) and when the SOPAS threshold value is exceeded and the alarm is triggered (b).

### 3.2 Testing program

More than 1500 experimental tests were performed, measuring the variation of the SOPAS along the fibers installed inside the physical model. The following conditions, which take into account different mobilized volumes and materials were reproduced:

1. No mechanical perturbation, to characterize the noise level of the system (N - Noise);
2. Rolling of one rock cobble (diameter equal to 4 cm) along the slope (S – Stone);
3. Rolling of a plastic cylinder (15 cm long and 5 cm in diameter) along the slope (C – Cylinder);

- 260 4. Release of different amounts of cobbles (13-25 pieces with an approximate diameter of 4-5 cm) along the slope  
261 (DF – Debris Flow);  
262 5. Rolling of one cobble (approximate diameter 4 cm) along the slope and final impact against a rockfall net equipped  
263 with fiber optic (RN – Rockfall Net).

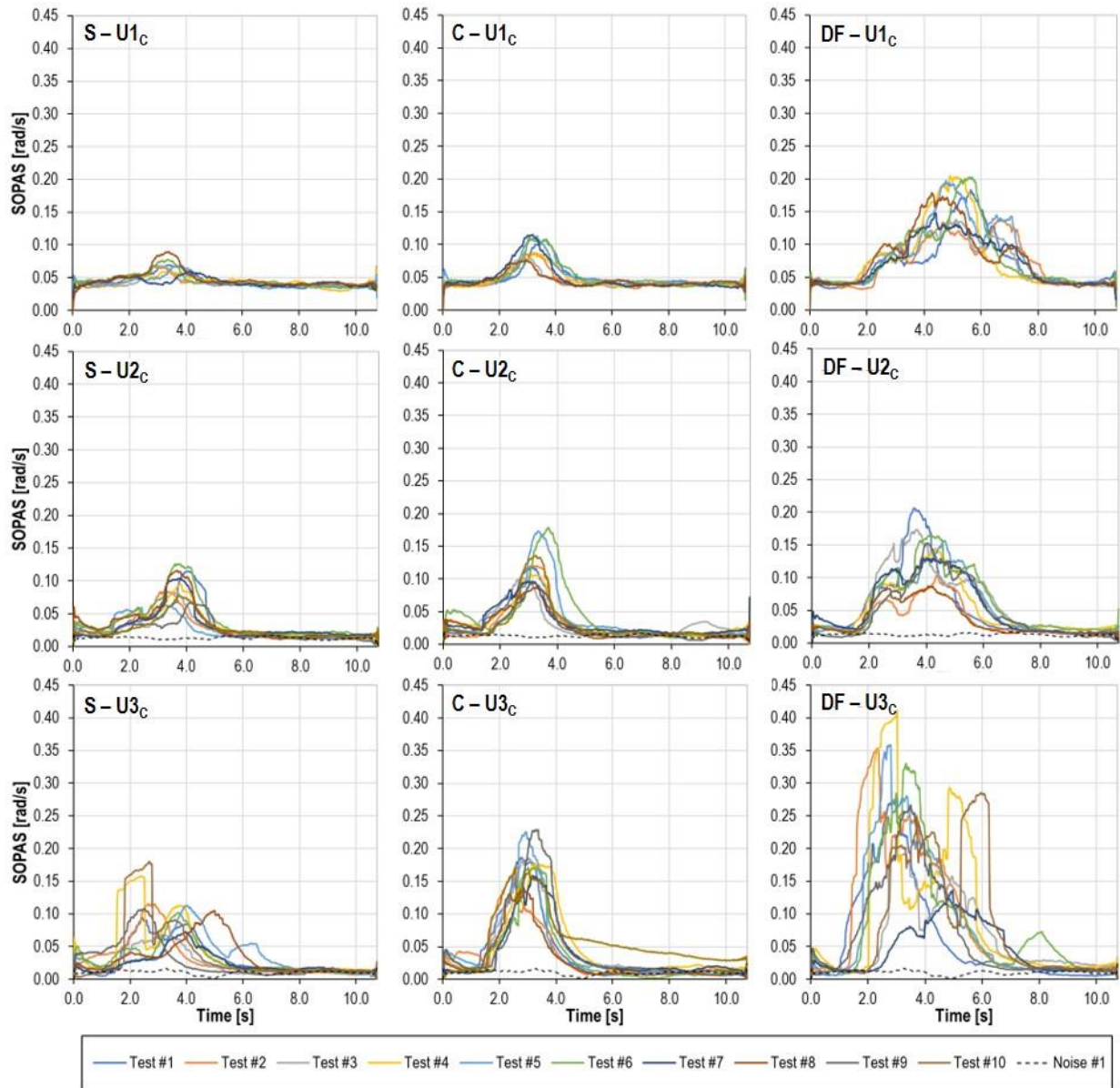
264 The assumption that has been made in this work is that the three different harmful events (debris flow, cylinder, single rock)  
265 are to be detected by the algorithm. The latter condition (DF) tries to reproduce, to scale and without the use of water, the  
266 occurrence of a mass movement along a slope or a channel which can be comparable to scale to the dynamic signal  
267 produced by a debris flow or a very dense avalanche (i.e. wet snow). The duration of the tests is variable, lasting from a  
268 minimum of 10.75 to a maximum of 21.5 s, in order to capture the whole evolution of the simulated events. The cylinder  
269 (C) and single rock (S) events have been selected with the aim to test the capability of the algorithm to detect them, as well  
270 as to understand the magnitude of the SOPAS in the different cases and to calibrate the algorithm parameters.

271 For each optical fiber tested ( $U_C$ ,  $U_L$ , and T), the measurements of the noise level of the system were performed at least  
272 three times, while the other conditions (S, C and DF) were tested at least ten times. This subset of 33 tests, which was  
273 repeated many times, was adopted to evaluate the possible variations of the noise levels over time and to easily identify  
274 possible sources of disturbances on the experimental setup.

275 Some long-term noise measurements (several hours) were also carried out to verify the presence of any deviation and  
276 potential anomalous behaviours of the noise over time. The test's repetition made it possible to create a sufficiently large  
277 database of signals which could be used to classify and distinguish the signals related to the emulated mass movements  
278 from all the further noisy features.

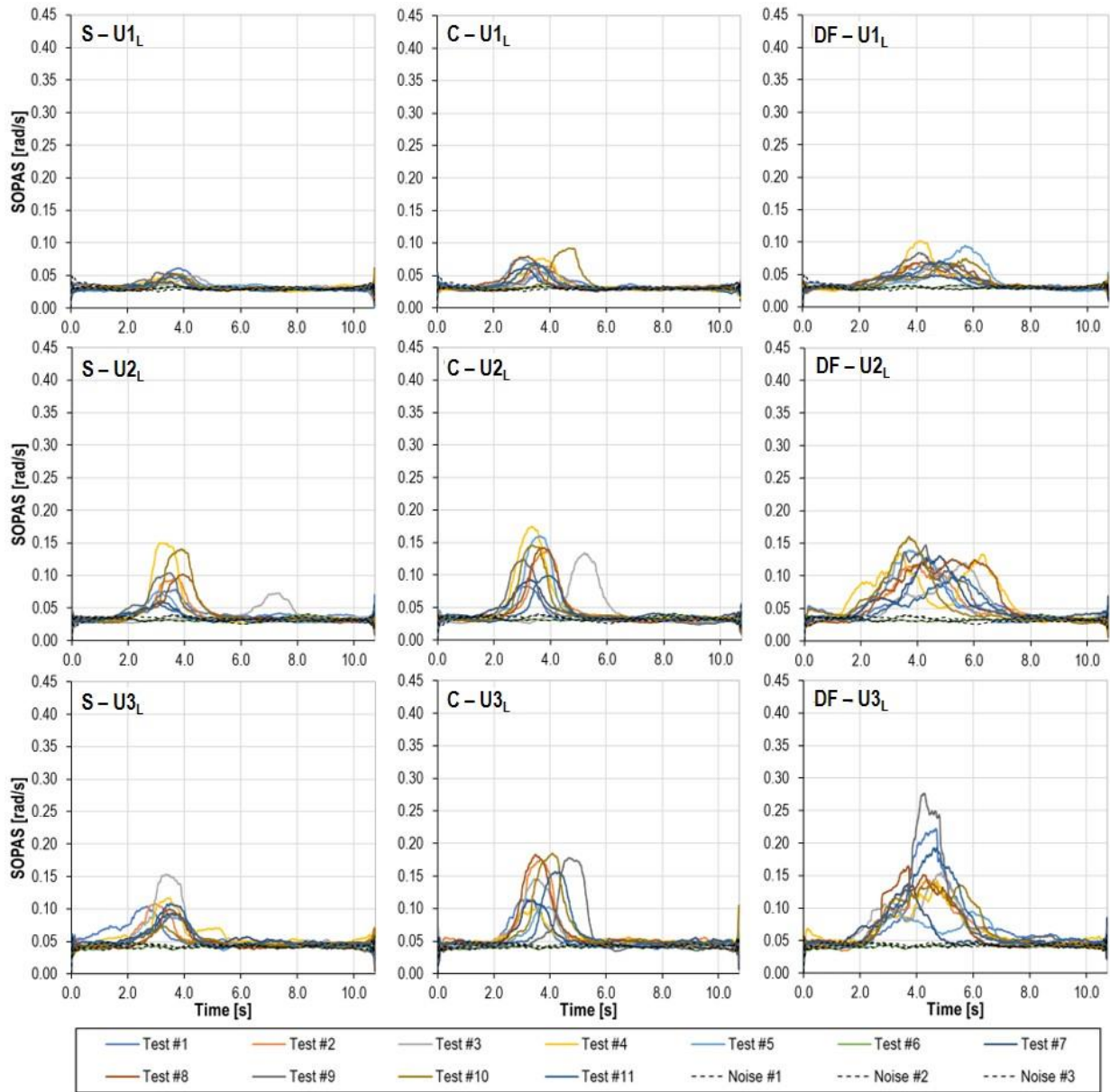
### 279 **3.3 Results of the laboratory tests**

280 The result of each test after the signals processing can be expressed through graphs showing the variations over time of  
281 the SOPAS angular speed in radians per second. Figures 7, 8 and 9 show the results of a series of tests both for the three  
282 different optical fibers configurations  $U_L$ ,  $U_C$  and T installed at different depths in the model (90, 50 and 10 mm) and for each  
283 test type carried out (S, C, DF and N). To allow a fruitful comparison, all scales' range are the same. Figure 10 shows the  
284 results for the tests carried out adopting the configurations RN1 and RN2.



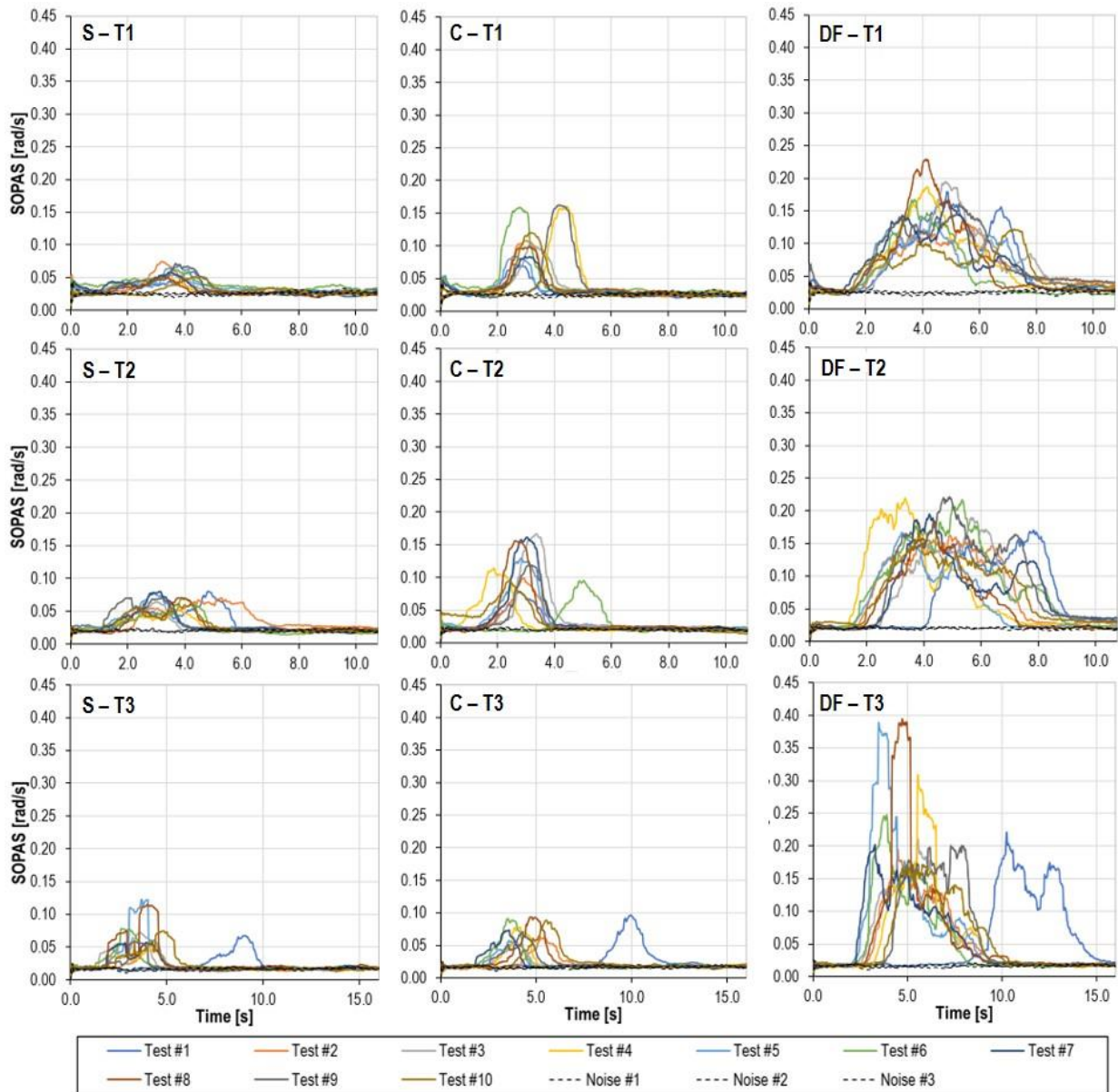
285  
 286  
 287  
 288  
 289

Figure 7 - Experimental results of 86 tests using the U<sub>c</sub> optical fibers configuration compared to noise measurements when available. The different codes identify the test carried out (S, C, DF) and the depth of the optical fibers in the model (1 = 90 mm, 2 = 50 mm, 3 = 10 mm).



290  
291  
292  
293  
294

Figure 8 – Experimental results of 108 tests using the U<sub>L</sub> optical fibers configuration compared to noise measurements. The different codes identify the test carried out (S, C, DF and N) and the depth of the optical fibers in the model (1 = 90 mm, 2 = 50 mm, 3 = 10 mm).



295  
296  
297  
298  
299

Figure 9 – Experimental results of 99 tests using the T optical fibers layout compared to noise measurements. The different codes identify the test carried out (S, C, DF and N) at a depth of 90 mm (1), 50 mm (2) and 10 mm (3) respectively.

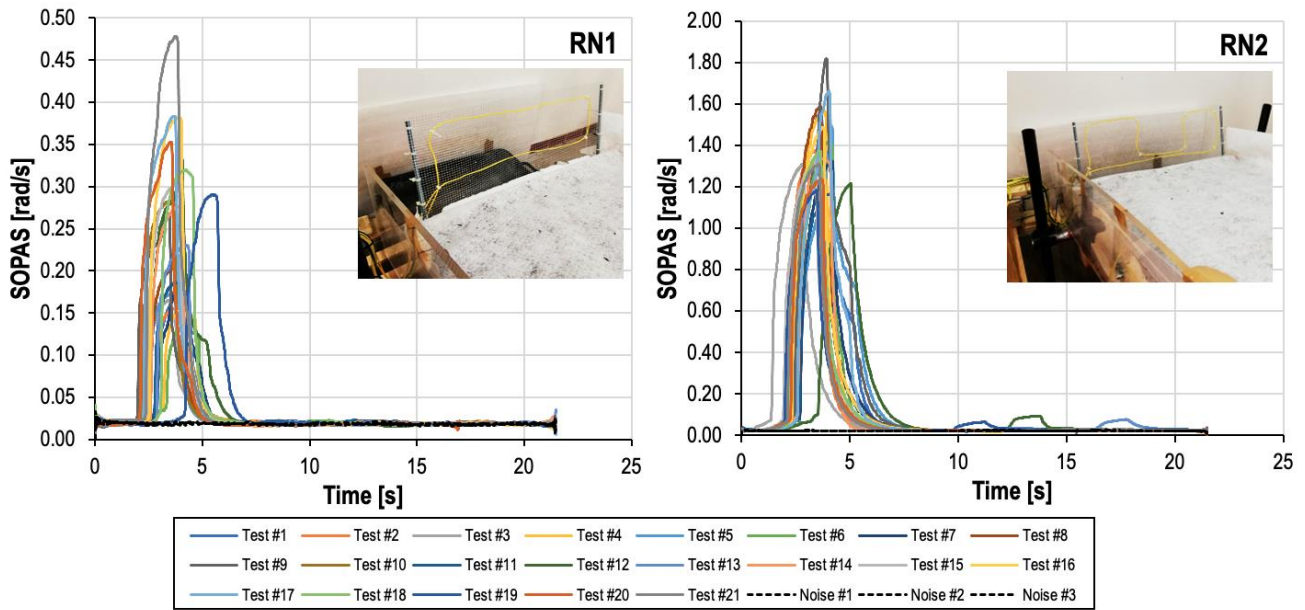


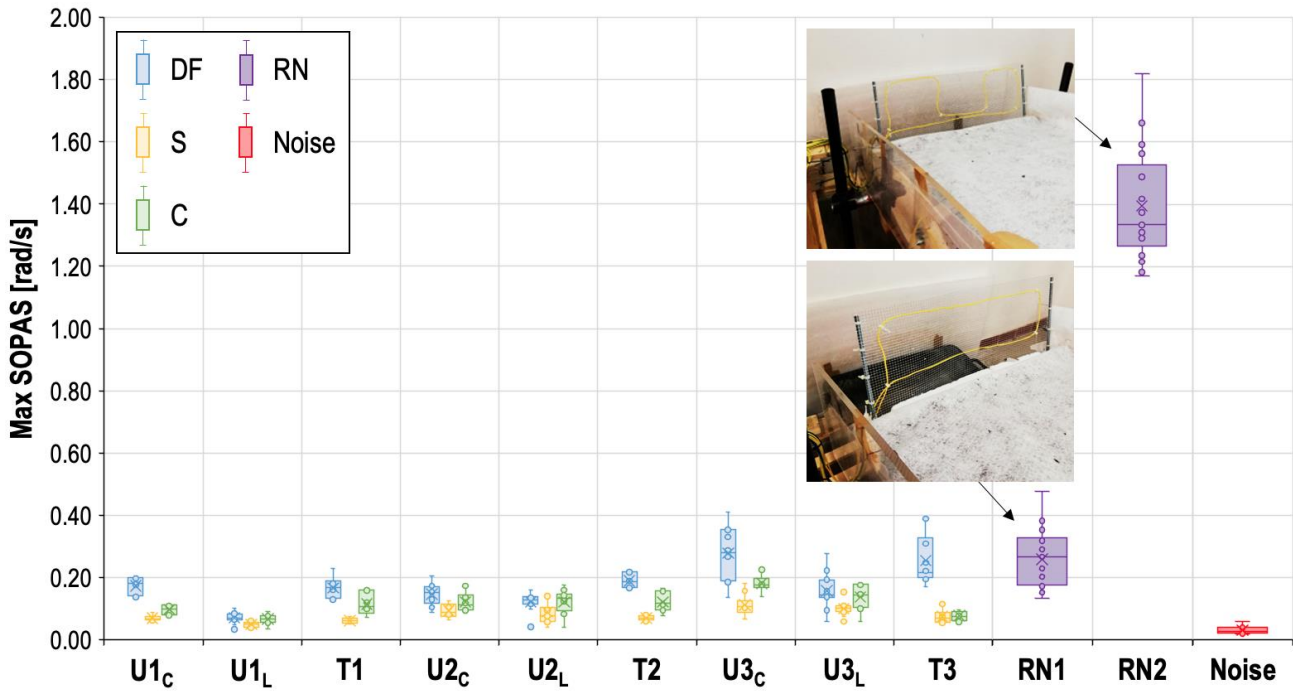
Figure 10 – Experimental results of 48 tests using the RN1 and RN2 optical fibers layout compared to noise measurements.

300  
301  
302  
303

304 All graphs show initially low SOPAS values, comparable to the measured noise levels, followed by a rapid increase up to  
305 one or more peaks, followed by a gradual decrease to the initial conditions when the simulated event is over. In general,  
306 the N simulations highlight noise levels (i.e. SOPAS values lower than 0.05 rad/s) that are comparable among the U<sub>L</sub>, U<sub>C</sub>,  
307 T and RN layouts tested without any significant differences.

308 The time series of S and C simulations are characterized by smoother patterns which reflect the dynamics of a single object  
309 rolling along the model. The DF time series are instead more complex and articulated since they reflect the dynamics of a  
310 granular media composed by macroscopic particles where collisions and rebounds take place in addition to rolling. It is also  
311 evident that the maximum SOPAS values were measured for the DF tests followed by the C and S tests for all the three  
312 different installation depths of the optical fibers. In some cases, as for instance the U<sub>2L</sub> and T3 layouts, the C and S tests  
313 have given comparable maximum SOPAS values. This can probably be related to the similar masses and velocities of the  
314 falling objects used in these tests.

315 The results of all the tests have been summarized in Figure 11 with the aim to have a glance at the statistical distribution of  
316 the test results. Here it can be seen that, given the randomness of the tests carried out, the results obtained in terms of  
317 maximum SOPAS change every time, however the order of magnitude of the maximum SOPAS recorded is always the  
318 same and in general higher than the recorded noise. This testifies the repeatability and reliability of the tests, despite the  
319 variability related to the testing conditions that shows that the DF condition, the most representative for in situ events, always  
320 stands out with respect to the others. In general, Figure 11 shows that the higher the depth of installation of the optical  
321 fibers, the lower the maximum SOPAS values measured during both S, C and DF tests. Also, the configurations RN1 and  
322 RN2 that simulate the rockfall barrier application are both effective, though the second one, due to its particular geometry,  
323 leads to much higher values of maximum recorded SOPAS.



324  
325

326 Figure 11 – Maximum SOPAS measured in all the tests carried out with the eleven different fibers optic layouts  $U_c$ ,  $U_L$ , T  
327 (at a depth of 90 mm (1), 50 mm (2) and 10 mm (3) respectively), RN1 and RN2, and at rest (noise).

328 Through the analysis of the SOPAS time series, it was also possible to estimate the average velocity of the falling objects  
329 along the experimental slope model. The values obtained are consistent with the time recorded during the experiments and  
330 appear to be in the range 0.9-1.9 m/s for the S and the C tests and 0.6-0.8 m/s for the DF tests. It is interesting to note that  
331 debris flows in alpine catchments are generally characterized by moderate propagation velocities of less than 10 m/s that  
332 can reach a lower bound values close to 1.5-2.0 m/s (Arattano and Marchi 2005; Coviello et al. 2019; Hurlimann et al. 2003;  
333 Schimmel et al. 2022).

334 The results obtained have shown that for all three optical fiber geometric layouts ( $U_c$ ,  $U_L$ , and T) and the different depths of  
335 installation tested, the system was able to sense and measure the SOP variations along the optical fibers caused by the  
336 vibration which propagates in the soil during the simulation of a mass movement at the laboratory scale. It is also shown  
337 that the detection occurs better for the fibers closer to the surface, however also the deepest ones are able to detect the  
338 event.

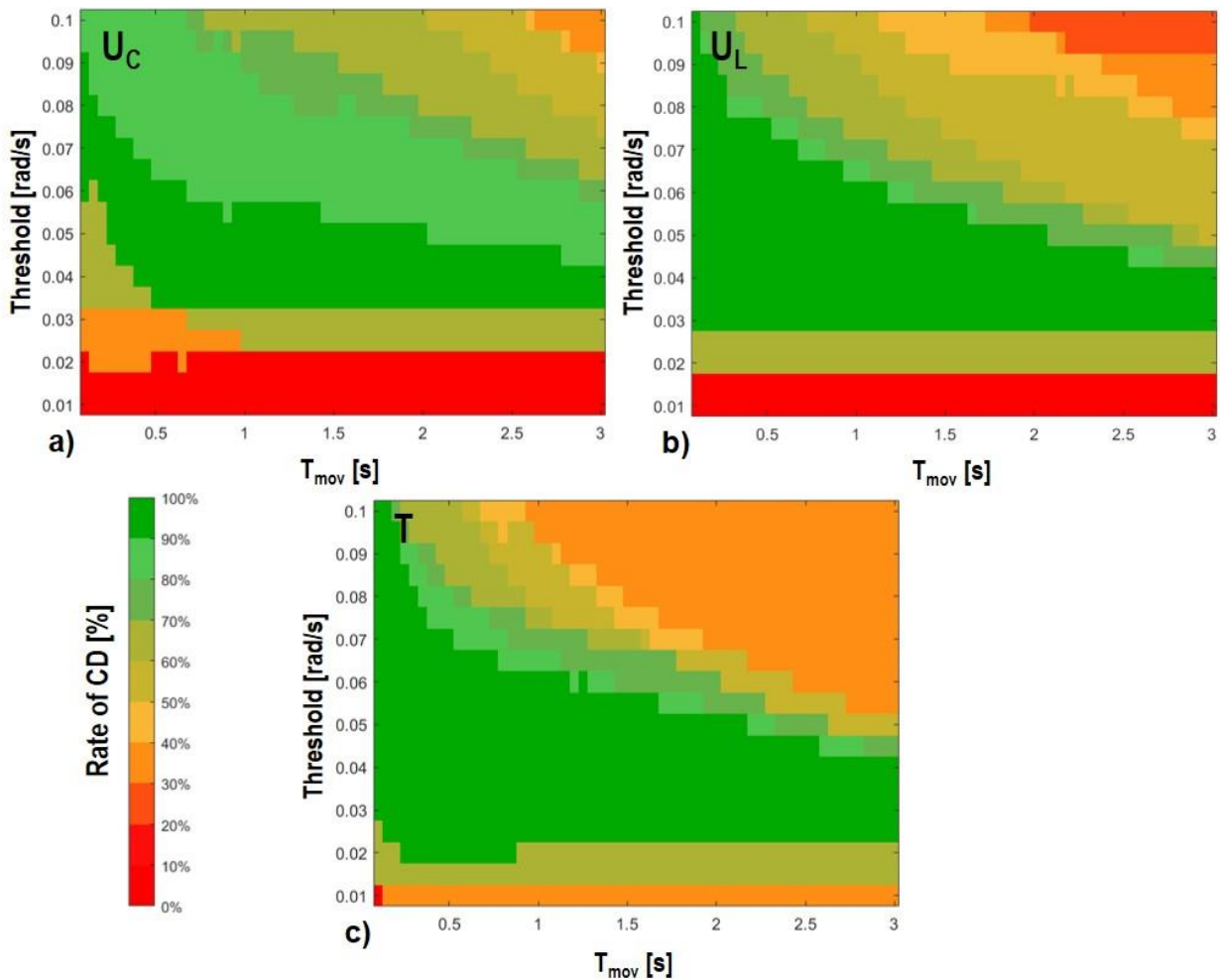
### 339 3.4 Validation of the algorithm

340 To assess the performance of the algorithm, all the data collected during the experimental campaign were processed  
341 through the application of the detection algorithm. The result obtained can be represented by specific contour plots which  
342 show, for each test type carried out (S, C, and DF), different combinations of  $T_{mov}$  and  $\omega_{th}$  values.

343 The graphs in Figure 12 summarize the behaviour of the algorithm for the three configurations of the fibers tested ( $U_c$ ,  $U_L$ ,  
344 and T) in all the 1500 tests performed. The green colour identifies a 100% correct detection (CD) rate on all fibers, regardless  
345 of their depth and for all the simulated mass movement events, while the red colour identifies pairs  $T_{mov}-\omega_{th}$  for which there

346 is a lack of identification (MDs and/or FAs). The lack of identification may depend either on the fact that the noise level is  
347 higher than the threshold or because at least one of the simulated events remains below the threshold for its entire duration.  
348 Yellow or orange colours denote intermediate conditions i.e., using these parameters the algorithm is able to correctly  
349 identify the simulated mass movement in the experimental model for some cases only. The layout of the plots, in terms of  
350 arrangement and distribution of the areas, suggests that a wide range of  $T_{mov}$ -  $\omega_{th}$  values can be used in the algorithm to  
351 obtain always a correct detection of the simulated events.

352 In particular, the system proved to be able to correctly recognize the mass movements from the condition of noise only and  
353 from further random disturbances simulated. This ability has been demonstrated for multiple combinations of the values  
354  $T_{mov}$ -  $\omega_{th}$  that, after an appropriate optimization, can be used in the real-time detection algorithm. For instance, by analyzing  
355 the overall results shown in Figure 12, values of  $T_{mov}$  in the range 1 – 2 s coupled with thresholds values between 0.035 and  
356 0.045 rad/s allowed for a correct triggering of the alarm regardless of the fibers installation depth. Even the position of the  
357 optical fibers in the model (central, lateral, or transversal) does not seem to be relevant for the detection of the simulated  
358 mass movements as shown in Figure 12. This has a very important implication for a future application of the system outside  
359 the laboratory. Although at the site scale it is realistic that the vibrations related to debris flows and snow avalanches may  
360 differ from those simulated in the laboratory, it is expected that the ratio between the environmental noise and the signal  
361 generated by these events may be similar since the optic fibers will be installed in the ground at depths greater than those  
362 tested in the laboratory. The determination of the  $T_{mov}$  and  $\omega_{th}$  values to be used on a real site, would require a recalibration  
363 to identify the SOPAS thresholds which could be sensibly higher.



364

365 Figure 12 - Contour plots showing the overall behaviour of the algorithm adopted to process the signals in terms of rate of  
 366 correct detection (CD) for the three configurations of the fibers tested  $U_C$  (a),  $U_L$  (b) and T (c) and for all the three depths of  
 367 installation (1 = 90 mm, 2 = 50 mm and 3 = 10 mm) with the variation of the time moving average ( $T_{mov}$ ) and the State of  
 368 Polarization Angular Speed (SOPAS) threshold  $\omega_{th}$

369 The previous observations are also extremely interesting for identifying the best installation geometry of the optic fibers: for  
 370 instance, by adopting a scheme where the optic fibers will be installed alongside of a channel (similar to the  $U_L$  scheme  
 371 previously described), it would be possible to correctly identify the occurrence of debris flows and snow avalanches as well  
 372 as to simplify the installation thus reducing the costs. Furthermore, this installation scheme along with the embedment of  
 373 the fibers into the ground will significantly minimize the possibility of damages to the sensing system (therefore minimizing  
 374 maintenance) since the cables will not interact directly with the masses moving along the gullies. In any case, should the  
 375 optical fibers be damaged, it will be possible to repair them easily on site through a partial replacement of the cables or  
 376 through a splicing.

#### 377 **4 Assessment of the technical and economic feasibility of the system**

378 The technical analysis of the proposed monitoring system based on optical fiber has highlighted excellent experimental  
 379 results after an appropriate optimization of the free parameters of the algorithm proposed for signals processing and the

380 subsequent generation of alarms. From a technological point of view, the results obtained so far have identified how the  
381 optical fibers polarimetric measurement constitutes an extremely promising technique in the geological and geotechnical  
382 fields since it has shown to be able to identify in a precise, prompt and rather simple way the polarimetric perturbations  
383 induced on the optical fibers by external forcings.

384 From an economic point of view, considering, for instance, an optical fiber loop of about 1 km installed along a mountain  
385 slope, the cost for the different devices (fiber optic cable, laser, polarimeter with an embedded real-time data analysis  
386 system, stand-alone power supply and radio node) is approximately around 25,000 €. Most of the cost is for the interrogator  
387 system, while the fiber optic cables would cost less than 2000 €. To this amount, the costs of the deployment of the optical  
388 fibers into the ground have to be added. These can vary depending on the ground to be excavated and the subsequent  
389 backfilling technique adopted and can be reduced if the fiber cable is fixed to the rock surface. An additional cost of  
390 approximately 5,000 € can be estimated to install the optical fiber at a depth of 5-10 cm, less in case of surface deployment.  
391 This will lead to a total cost of around 30,000 € for the deployment and installation of an EWS system based on the proposed  
392 technique.

393 The estimated cost is slightly higher than typical installation costs for EWS systems based on "discrete" sensors (such as  
394 trigger lines, ultrasonic, seismic, or infrasonic sensors, etc.). However, it is believed that the technical advantages that is  
395 acquired with the use of a DFOS system can compensate for the higher installation costs. The possibility to measure data  
396 over large areas where the debris flows or the avalanches propagates and to transfer this information through fiber optic  
397 cables at distance from the monitored area is a peculiar aspect. Another value-add of the technique is the possibility to  
398 measure the velocity of the snow and debris masses moving along channels and slopes by using different optical fiber  
399 circuits placed at different positions along the channel coupled with an optical switch (i.e. using the same interrogator). The  
400 optical switch allows to interrogate sequentially and in real time all the circuits to identify the passage of a snow or debris  
401 mass in different channel sections. The signal retrieved by each circuit combined with the specific position along the slope  
402 may be then used to calculate the velocity of the moving mass. Finally, the reliability of the detection algorithm and the  
403 reduction of false alarms could also increase safety along roads or railways reducing unnecessary closure to the transit of  
404 the infrastructure or, worse, the direct involvement of the users of the infrastructures. There are also potential long-term  
405 savings from reduced maintenance in comparison with other systems (e.g. no need to adjust pendulums height for winter  
406 and summer detection, less elements at risk of damages during strong events).

## 407 **5 Conclusions**

408 A new system, called Optialp, to detect the propagation of debris flows and snow avalanches along mountain gulleys and  
409 generate alert signals to be used in an EWS was here presented. It is applicable to mountain gullies where debris flow  
410 phenomena and/or snow avalanches occur repeatedly over time with similar intensity and kinematics as well as on rockfall  
411 hazard mitigation structures. The proposed system is reliable, simple, and requires quite low-cost devices.

412 The main focus of the work was to demonstrate the effectiveness of the system by presenting the results of an extensive  
413 laboratory activity aimed at evaluating the feasibility of the use of a new DFOS system to detect the propagation of simulated  
414 mass movements by measuring in real-time the polarization variations along the optical fibers. The results obtained have

415 identified how the measurement of optical fibers polarimetric variations can identify, at least at the laboratory scale, in a  
416 precise and rather simple way the polarimetric perturbations induced on the optical fibers by external forcings. The  
417 performance of the system for the identification of the simulated mass movements in the model is satisfactory after an  
418 appropriate optimization of the free parameters ( $T_{mov}$  and  $\omega_{th}$ ) which govern the algorithm developed for the processing of  
419 the signals and for the subsequent generation of alarms. At the same time, the algorithm characterized by a high speed of  
420 response has shown a minimization of the probability of occurrence of false alarms or missed detection. The algorithm is  
421 embedded into a prototype of the fiber optic interrogator capable to perform the real-time analysis of the acquired data and  
422 to generate an alarm signal whenever the threshold value of the state of polarization angular speed ( $\omega_{th}$ ) is exceeded.

423 The examination of the economic feasibility of the system highlighted slightly higher construction and installation costs with  
424 respect to existing alternatives based on "discrete" sensors. Nevertheless, this can be considered acceptable considering  
425 the advantage of being able to measure and detect mass movements along large sectors of slopes or catchment basins. It  
426 is believed that the technical advantage that is acquired with the use of Optialp can completely compensate for these initial  
427 slightly higher costs. Moreover, the possibility to carry out a distributed measurement, extending the sensing system for  
428 lengths even greater than few kilometers, rather than the use of discrete sensors for large-scale linear infrastructures  
429 determines a better and higher mitigation of the risks caused by debris flows and avalanches.

430 The laboratory results suggest that the optical fibers embedded into the ground along one or more sections of the channels  
431 where the debris flows or snow avalanches propagate can be used as a novel distributed detection and early warning  
432 system, improving the current technology which typically is based on discrete monitoring points and sensors. The Optialp  
433 system could then represent a valid alternative to the existing state-of-the-art monitoring techniques, both in the geotechnical  
434 and optical fields. The instantaneous and real-time response and the high sensitivity of optical fibers coupled with a high  
435 wear resistance of the cables embedded into the ground and relative ease of installation are all value adds. From the optical  
436 point of view, the advantages of the polarimetric technique adopted for the Optialp system are the simpler and therefore  
437 less expensive equipment than other DFOS based on OTDR, OFDR and FBG as well as the simpler processing required  
438 to identify debris flows and avalanches.

439 Further experimental activity will be devoted to testing the system in a relevant environment i.e., a gully where debris flows  
440 and/or avalanches usually occur, to confirm the satisfactory results obtained at the laboratory scale and verify the robustness  
441 of the installation. The use of artificial intelligence based on neural networks could also be investigated to automatically  
442 identify the change of polarization along the fibers related to the occurrence of real debris flows and avalanches and to  
443 distinguish among different events, enabling not only a further reduction of the false alarms and missed detection cases but  
444 also a classification of the events.

445

446

## 447 **Acknowledgements**

448 The work described in this paper was partially funded by Regione Piemonte under the P.O.R. FESR 2014/2020 – Asse I –  
449 Azione I.1b.I.2 Bando PASS "OPTIALP Project". The authors would also like to thank Yihan Du, Daniele Rosi and Filippo  
450 Vigna for their help in the experimental setup construction and the execution of the testing program.

451 **Author contributions:**

452 Conceptualization: Marco Barla; Methodology: Marco Barla, Roberto Gaudino, Alessandra Insana; Formal analysis and investigation:  
453 Francesco Antolini, Alessandra Insana, Giuseppe Rizzelli Martella, Saverio Pellegrini; Experiments: Francesco Antolini, Marco Barla,  
454 Alessandra Insana, Giuseppe Rizzelli Martella, Saverio Pellegrini; Writing - original draft preparation: Francesco Antolini; Writing - review  
455 and editing: Marco Barla, Alessandra Insana; Funding acquisition: Santina Aiassa, Marco Barla; Resources: Santina Aiassa, Marco  
456 Barla, Roberto Gaudino, Alessandra Insana; Supervision: Marco Barla, Roberto Gaudino.

457

458 **Competing Interests:**

459 The authors submitted to patenting on 07/12/2022 the system described in the paper (Priority number 102022000025158).

460

## 461 **References**

- 462 Aaron J, Spielmann R, McArdell BW, Graf C (2023) High-frequency 3D LiDAR measurements of a debris flow: A novel  
463 method to investigate the dynamics of full-scale events in the field. *Geophys Res Lett* 50, e2022GL102373.  
464 <https://doi.org/10.1029/2022GL102373>
- 465 Antolini F, Aiassa S, Barla M (2019) An Early Warning System for Debris Flows and Snow Avalanches. In: Calvetti F,  
466 Cotecchia F, Galli A, Jommi C (eds) *Geotechnical Research for Land Protection and Development*. CNRIG 2019. Lecture  
467 Notes in Civil Engineering, vol 40. Springer, Cham
- 468 Arattano M, Marchi L (2005) Measurements of debris flow velocity through cross-correlation of instrumentation data. *Nat*  
469 *Hazard Earth Sys* 5(1):137-142. [https://doi.org/doi\\_10.5194/nhess-5-137-2005](https://doi.org/doi_10.5194/nhess-5-137-2005)
- 470 Aufleger M, Conrad M, Goltz M, Perzmaier S, Porras P (2007) Innovative dam monitoring tools based on distributed  
471 temperature measurement. *Jordan J. Civ. Eng* 1(1):29-37
- 472 Bao X, Wang Y (2021) Recent advancements in Rayleigh scattering-based distributed fiber sensors. *Advanced devices &*  
473 *instrumentation*. <https://doi.org/10.34133/2021/869657>
- 474 Beck YL, Khan AA, Cunat P, Guidoux C, Artières O, Mars J, Fry JJ (2010) Thermal monitoring of embankment dams by  
475 fiber optics. In: *Proceedings of the 8th ICOLD European Club Symposium, Innsbruck, Austria, 22-23 September 2010*, pp  
476 444-448
- 477 Belli G, Walter F, McArdell B, Gheri D, Marchetti E (2022) Infrasonic and seismic analysis of debris-flow events at Illgraben  
478 (Switzerland): Relating signal features to flow parameters and to the seismo-acoustic source mechanism. *Journal of*  
479 *Geophysical Research: Earth Surface* 127, e2021JF006576. <https://doi.org/10.1029/2021JF006576>
- 480 Beniston M, Stoffel M, Hill M (2011) Impacts of climatic change on water and natural hazards in the Alps: can current water  
481 governance cope with future challenges? Examples from the European “ACQWA” project. *Environmental Science & Policy*,  
482 14(7):734-743. <https://doi.org/10.1016/j.envsci.2010.12.009>
- 483 Bertolo P, Wicczorek GF (2005) Calibration of numerical models for small debris flows in Yosemite Valley, California, USA.  
484 *Nat Hazards Earth Syst Sci* 5(6):993–1001. <https://doi.org/10.5194/nhess-5-993-2005>
- 485 Bigano A, Pauli F (2007) Dimensioni socio-economiche, costi dell’inflazione e strategie di adattamento per l’impatto del  
486 cambiamento climatico sul sistema idrogeologico italiano. In Report prepared for the APAT Workshop on “Cambiamenti  
487 climatici e dissesto idrogeologico: scenari futuri per un programma nazionale di adattamento”, Napoli (pp. 9-10)
- 488 Bolognini G, Soto MA, Di Pasquale F (2009) Fiber-optic distributed sensor based on hybrid Raman and Brillouin scattering  
489 employing multiwavelength Fabry–Pérot lasers. *IEEE Photonics Technology Letters* 21(20):1523-1525

490 Butler DR, Malanson GP (1992) Effects of terrain on excessive travel distance by snow avalanches. Northwest science  
491 66(2):77-85.

492 Coviello V, Arattano M, Comiti F, Macconi P, Marchi L (2019) Seismic characterization of debris flows: Insights into energy  
493 radiation and implications for warning. *Journal of Geophysical Research: Earth Surface* 124:1440–1463.  
494 <https://doi.org/10.1029/2018JF004683>

495 Edme P, Paitz, P, Walter F, van Herwijnen A, Fichtner A (2023) Fiber-optic detection of snow avalanches using  
496 telecommunication infrastructure. arXiv preprint arXiv:2302.12649

497 EEA (2017) Climate change adaptation and disaster risk reduction in Europe 2017. EEA Report No 15/2017, Publications  
498 Office of the European Union, Luxembourg, 2017, pp 172. <https://doi.org/10.2800/938195>

499 Fichtner A, Klaasen S, Thrastarson S, Cubuk-Sabuncu Y, Paitz P, Jonsdottir K (2022) Fiber-optic observation of volcanic  
500 tremor through floating ice-sheet resonance. *The Seismic Record* 2(3):148-155. <https://doi.org/10.1785/0320220010>

501 Forman PR, Jahoda FC (1988) Linear birefringence effects on fiber-optic current sensors. *Appl. Opt.* 27(15):3088-3096.  
502 <https://doi.org/10.1364/AO.27.003088>

503 Gauer P (2014) Comparison of avalanche front velocity measurements and implications for avalanche models. *Cold regions  
504 science and technology* 97:132-150. <https://doi.org/10.1016/j.coldregions.2013.09.010>

505 Gauer P, Kern M, Kristensen K, Lied K, Rammer L, Schreiber H (2007) On pulsed Doppler radar measurements of  
506 avalanches and their implication to avalanche dynamics. *Cold Regions Science and Technology* 50(1-3):55-71.  
507 <https://doi.org/10.1016/j.coldregions.2007.03.009>

508 Havens S, Marshall HP, Johnson JB, Nicholson B (2014) Calculating the velocity of a fast-moving snow avalanche using  
509 an infrasound array. *Geophysical Research Letters* 41(17):6191-6198. <https://doi.org/10.1002/2014GL061254>

510 Hong CY, Zhang YF, Zhang MX, Leung LMG, Liu LQ (2016) Application of FBG sensors for geotechnical health monitoring,  
511 a review of sensor design, implementation methods and packaging techniques. *Sensors and Actuators A: Physical* 244:184-  
512 197. <https://doi.org/10.1016/j.sna.2016.04.033>

513 Hudson TS, Baird AF, Kendall JM, Kufner SK, Brisbourne AM, Smith AM, Butcher A, Chalari A, Clarke A (2021) Distributed  
514 Acoustic Sensing (DAS) for natural microseismicity studies: A case study from Antarctica. *J. Geophys. Res.: Solid Earth*  
515 126, e2020JB021493. <https://doi.org/10.1029/2020JB021493>

516 Hungr O, Leroueil S, Picarelli L (2014) The Varnes classification of landslide types, an update. *Landslides* 11:167-194.  
517 <https://doi.org/10.1007/s10346-013-0436-y>

518 Hurlimann M, Rickenmann D, Graf C (2003) Field and monitoring data of debris-flow events in the Swiss Alps. *Canadian*  
519 *Geotechnical Journal* 40:161–175. <https://doi.org/10.1139/t02-087>

520 Hurlimann M, Coviello V, Bel C, Guo X, Berti M, Graf C, Hübl J, Miyata S, Smith JB, Yin HY (2019) Debris-flow monitoring  
521 and warning: Review and examples. *Earth-Science Reviews* 199, 102981. <https://doi.org/10.1016/j.earscirev.2019.102981>

522 Inaudi D (2014) Sensing solutions for assessing the stability of levees, sinkholes and landslides. In: *Sensor Technologies*  
523 *for Civil Infrastructures*; Elsevier: Amsterdam, The Netherlands, 2014; Volume 1

524 Insana A, Beroya-Eitner MA, Barla M, Zachert H, Žlender B, van Marle M, Kalsnes B, Bracko T, Pereira C, Prodan I,  
525 Szymkiewicz F, Löfroth H (2021) Climate Change Adaptation of Geo-Structures in Europe: Emerging Issues and Future  
526 Steps. *Geosciences* 11(12), 488.

527 IPCC (2023) Climate change 2023. Synthesis Report. The Intergovernmental Panel on Climate Change, 169 pp.  
528 <https://doi.org/10.59327/IPCC/AR6-9789291691647>

529 Itakura Y, Inaba H, Sawada T (2005) A debris-flow monitoring devices and methods bibliography. *Nat. Hazards Earth Syst.*  
530 *Sci.* 5(6):971-977. <https://doi.org/10.5194/nhess-5-971-2005>, 2005.

531 Iverson RM (1997) The physics of debris flows. *Rev Geophys* 35(3):245–296. <https://doi.org/10.1029/97RG00426>

532 Jakob M (2005) A size classification for debris flows. *Engineering geology* 79(3-4):151-161.  
533 <https://doi.org/10.1016/j.enggeo.2005.01.006>

534 Johansson S, Farhadiroushan M, Parker T (2000) Application of fibre-optics systems in embankment dams for temperature,  
535 strain and pressure measurements-Some comparisons and experiences. In: *Transactions of the International Congress on*  
536 *Large Dams*. 2000. p. 1125-1146

537 Kogelnik H, Winzer PJ (2012) Modal birefringence in weakly guiding fibers. *Journal of Lightwave Technology* 30(14):2240–  
538 2245. <https://doi.org/10.1109/JLT.2012.2193872>

539 Leonardi A, Pirulli M, Barbero M, Barpi F, Borri-Brunetto M, Pallara O, Segor V (2021) Impact of Debris Flows on Filter  
540 Barriers: Analysis Based on Site Monitoring Data. *Environmental & Engineering Geoscience* 27(2):195–212.  
541 <https://doi.org/10.2113/eeg-d-20-00013>

542 Lloret S, Rastogi P, Thévenaz L, Inaudi D (2003) Measurement of dynamic deformations using a path-unbalance Michelson-  
543 interferometer-based optical fiber sensing device. *Opt. Eng.* 42(3):662–669

544 Marchi L, Arattano M, Deganutti AM (2002) Ten years of debris-flow monitoring in the Moscardo Torrent (Italian Alps).  
545 *Geomorphology* 46(1-2):1-17. [https://doi.org/10.1016/S0169-555X\(01\)00162-3](https://doi.org/10.1016/S0169-555X(01)00162-3)

546 McClung D, Schaerer PA (2006). The avalanche handbook. The Mountaineers Books

547 Michlmayr G, Chalari A, Clarke A, Or D (2017) Fiber-optic high-resolution acoustic emission (AE) monitoring of slope failure.  
548 Landslides 14(3):1139-1146. <https://doi.org/10.1007/s10346-016-0776-5>

549 Motil A, Bergman A, Tur M (2016) State of the art of Brillouin fiber-optic distributed sensing. Optics & Laser Technology  
550 78:81-103. <https://doi.org/10.1016/j.optlastec.2015.09.013>

551 Nagl G, Hübl J, Kaitna R (2022). Stress anisotropy in natural debris flows during impacting a monitoring structure. Landslides  
552 19:211–220. <https://doi.org/10.1007/s10346-021-01779-2>

553 Olivero M, Insana A, Vallan A, Gaudino R, Barla M, Perrone G (2018) Fibre Bragg Gratings Monitoring in a Pilot Project of  
554 an Energy Tunnel, 20th Italian National Conference on Photonic Technologies (Fotonica 2018), Lecce, Italy, 2018, pp. 1-4.  
555 <https://doi.org/10.1049/cp.2018.1649>

556 Pelfini M, Santilli M (2008) Frequency of debris flows and their relation with precipitation: A case study in the Central Alps,  
557 Italy. Geomorphology 101(4):721-730

558 Pellegrini S, Rizzelli G, Barla M, Gaudino R (2023) Algorithm Optimization for Rockfalls Alarm System Based on Fiber  
559 Polarization Sensing. IEEE PHOTONICS JOURNAL 15(3):1-9. <https://doi.org/10.1109/JPHOT.2023.3281670>

560 Pellegrini, S, Rizzelli, G., Barla M., Gaudino R. (2024) Polarization-Based Fiber Optic System for Debris Flow Early Warning:  
561 On-Field Demonstration. IEEE PHOTONICS JOURNAL 16(3): 1-8. <https://doi.org/10.1109/JPHOT.2024.3403159>

562 Prochaska AB, Santi PM, Higgins JD, Cannon SH (2008) A study of methods to estimate debris flow velocity. Landslides  
563 5(4):431-444. <https://doi.org/10.1007/s10346-008-0137-0>

564 Qin, J.-Q., Yin J.-H., Zhu Z.-H., Tan D.-Y. (2020) Development and application of new FBG mini tension link transducers  
565 for monitoring dynamic response of a flexible barrier under impact loads. Measurement 153 (2020) 107409.  
566 <https://doi.org/10.1016/j.measurement.2019.107409>

567 Rammer L, Kern MA, Gruber U, Tiefenbacher F (2007) Comparison of avalanche-velocity measurements by means of  
568 pulsed Doppler radar, continuous wave radar and optical methods. Cold Regions Science and Technology 50(1-3):35-54.  
569 <https://doi.org/10.1016/j.coldregions.2007.03.014>

570 Sass O, Oberlechner M (2012) Is climate change causing increased rockfall frequency in Austria? Natural Hazards and  
571 Earth System Sciences 12(11):3209-3216. <https://doi.org/10.5194/nhess-12-3209-2012>

572 Schenato L (2017) A review of Distributed Fibre Optic Sensors for Geo-Hydrogeological applications. Appl. Sci. 7(9):896.  
573 <https://doi.org/10.3390/app7090896>

- 574 Schimmel A, Coviello V, Comiti F (2022) Debris flow velocity and volume estimations based on seismic data. *Nat. Hazards*  
575 *Earth Syst. Sci.* 22:1955–1968. <https://doi.org/10.5194/nhess-22-1955-2022>
- 576 Schweizer J, Bartelt P, van Herwijnen A (2021) Chapter 12 - Snow avalanches. In: *Snow and ice-related hazards, risks,*  
577 *and disasters (Second Edition)*, edited by: Haeberli, W. and White- man, C., Elsevier, 377–416.  
578 <https://doi.org/10.1016/B978-0-12-394849-6.00012-3>
- 579 Stocker TF et al. (eds) (2013) *Climate Change 2013: The Physical Science Basis*. Cambridge Univ. Press, 2013
- 580 Stoffel M, Huggel C (2012) Effects of climate change on mass movements in mountain environments. *Progress in physical*  
581 *geography* 36(3):421-439. <https://doi.org/10.1177/0309133312441010>
- 582 Tan D. -Y., Yin J.-H., Qin J.-Q., Zhu Z.-H., Feng W.-Q. (2020) Experimental study on impact and deposition behaviours of  
583 multiple surges of channelized debris flow on a flexible barrier. *Landslides* (2020) 17:1577–1589.  
584 <https://doi.org/10.1007/s10346-020-01378-7>
- 585 Thüring T, Schoch M, van Herwijnen A, Schweizer J (2015) Robust snow avalanche detection using supervised machine  
586 learning with infrasonic sensor arrays. *Cold Regions Science and Technology* 111:60-66
- 587 Ulivieri G, Marchetti E, Ripepe M, Chiambretti I, De Rosa G, Segor V (2011) Monitoring snow avalanches in Northwestern  
588 Italian Alps using an infrasound array. *Cold Regions Science and Technology* 69(2-3):177-183
- 589 Wang H, Guo J-K, Mo H, Zhou X, Han Y (2023). Fiber Optic Sensing Technology and Vision Sensing Technology for  
590 Structural Health Monitoring. *Sensors* 23(9), 4334. <https://doi.org/10.3390/s23094334>
- 591 Zhu HH, Shi B, Zhang CC (2017) FBG-Based Monitoring of Geohazards: Current Status and Trends. *Sensors* 17(3), 452.  
592 <https://doi.org/10.3390/s17030452>